Int. J. Electrochem. Sci., 13 **(2018)** 7193 – 7205, doi: 10.20964/2018.07.72

International Journal of ELECTROCHEMICAL SCIENCE
www.electrochemsci.org

Synthesis and Characterization of Ni-Co Electrocatalyst for Hydrogen Evolution Reaction in Acidic Media

Yufang Yang[*], *Huan Yang, Changjin Liang, Xun Zhu*

School of Material Science and Engineering, Hanshan Normal University, Chaozhou 521041, China
[*]E-mail: zzyufang@163.com

Received: 23 February 2018 / *Accepted:* 7 May 2018 / *Published:* 5 June 2018

Ni-Co was electrodeposited onto titanium substrates, as a non-noble metal electrocatalyst. The surface morphology and microstructure were observed by scanning electron microscopy (SEM) and X-ray diffraction (XRD). The electrocatalytic properties of Ni-Co for hydrogen evolution reaction (HER) in acid solution were investigated by using cathodic polarization, Tafel curves, electrochemical impedance spectroscopy (EIS), cyclic voltammetry and chronoamperometry. The surface is rough with uniform, compact and fine spherical particles on it. The Ni-Co is a face centered cubic (fcc) solid solution. The results show that HER on Ni-Co electrodes takes place by the Volmer- Heyrovsky mixing mechanism. With an increase of Co content in the electrode, and with the increase of sulfuric acid concentration and temperature, the cathodic polarization and the electrochemical reaction resistance of HER decrease, the exchange current density increases, and the electrocatalytic activity of Ni-Co for HER is enhanced. The $Ni_{64.4}Co_{35.6}$ shows the highest electrocatalytic activity for HER, with better stability and corrosion resistance. It can be used as an active, stable and inexpensive electrocatalyst for the HER in acidic media.

Keywords: Ni-Co alloys; Electrodeposition; Electrocatalysis; Hydrogen evolution reaction; Acidic media

1. INTRODUCTION

Hydrogen (H_2) is not only a green, efficient, and nonpolluting fuel, but also is widely utilized in the production of food, chemicals and fertilizers. Hydrogen has attracted worldwide attention as a secondary energy carrier. The most commonly used method for large-scale industrial hydrogen production is fossil fuel conversion. However, this method will lead to the emission of carbon dioxide, carbon monoxide, and other gas pollutants to the environment, and there are uncertainties of future energy supplies. The production of hydrogen from water is considered to be a better choice. Both photoelectrochemical and electrochemical water splitting to high scale H_2 production offer a promising

route [1]. For the photoelectrochemical water splitting method, an efficient, cheap and environmentally friendly water oxidising compound is highly desirable for artificial photosynthetic systems [2-4] toward hydrogen production. Therefore, the electrocatalytic hydrogen evolution reaction (HER) is a more effective way to realize the transformation of electric energy to chemical energy. It is not only an important means to realize large- scale production of hydrogen, but is also important for hydrogen production by electrolysis of water and fuel cell applications [5-9]. As an HER material, it is required to have a large active surface area, good electrochemical stability, good conductivity, low hydrogen evolution overpotential, good electrocatalytic activity and high corrosion resistance. Noble metals Pt and Pd, with the advantage of low hydrogen evolution overpotential, were earlier applied as electrocatalytic HER materials. However, due to being expensive and rare, they are not conducive to industrial large-scale applications [10-14]. Non-noble metal Ni and Ni-based electrodes show higher electrocatalytic activity for hydrogen evolution [10,14-27], and are gaining greater attention from the researchers. These higher electrocatalytic activity Ni-based HER materials include Ni-based composite [14-15], Ni-Mo [16-18], Ni-W [19], Ni-Co [20-21], Ni-Co-Mo [22-24], Ni-Co-Y [25], Ni-Co-Sn [26], Co-Ni-Fe-C [27] and other Ni-based alloys. As Ni and Co have the same electronic layer structure, Ni-Co alloy shows good synergy in electrocatalytic hydrogen evolution performance. It not only exhibits better electrocatalytic activity for HER than single-metal Ni and Co, but also has a lower hydrogen evolution overpotential than the smooth Pt electrode. There are several scientific reports available on the electrocatalytic HER of binary Ni-Co alloys [10,20-21,28] and more papers of ternary Ni-Co alloys [22-27] showing improved catalytic activity. For example, Ni-Co alloys electrodeposited on aluminium net [21], macroporous Ni- Co electrodes [20], three-dimensional hierarchical nickel-cobalt alloy coating [28] and the ordered meso-porous Ni-Co alloys [10] all manifest higher electrocatalytic activity toward the HER in the alkaline solution. However, it is probably due to the consideration of the stability and corrosion resistance of Ni-Co alloys in acidic medium; few papers are available on HER in the acidic solution. It is known that the high overpotentials for HER hinder the high scale hydrogen production by means of alkaline water electrolysis systems [29], and their main disadvantages are chiefly related to the low efficiency and high energy consumption [30]. In this paper, Ni-Co electrocatalyst material is fabricated by electrodeposition on a titanium substrate. Its electrocatalytic properties towards HER in acid solution were assessed by cathodic polarization curves, cyclic voltammetry, electrochemical impedance spectroscopy (EIS) and chronoamperometry.

2. EXPERIMENTAL

2.1 Preparation of Ni-Co electrocatalyst

Analytical grade chemical reagents were used for all experiments. The Ni-Co electrocatalyst was electrodeposited using a 250ml rectangular cell with agitated electrolyte. The high purity titanium sheet with the exposed area of 2.5cm×4cm was used as the cathode, and the electrolytic nickel was used as the anode, spaced 5cm apart from the cathode. The non-working surface of the cathode was sealed with cellophane, and the area ratio of anode to cathode was kept at 2. Prior to deposition, the titanium substrate was pretreated. The sequence of pretreatment is as follows; polished with silicon carbide emery paper; degreased in acetone; activated in the mixed dilute solution of 10 wt% HNO_3 and

10 wt% HF, and then washed with deionized water. The electrolyte was composed of 45g/l $NiCl_2 \cdot 6H_2O$, 100g/l $NiSO_4 \cdot 6H_2O$, 20g/l $CoSO_4 \cdot 7H_2O$, 30g/l H_3BO_3, 4g/l saccharin and 0.1g/l sodium dodecyl sulfate, and the Ni^{2+}/ Co^{2+} theoretical mol ratio in the precursor solution was about 8.01. All the plating solutions were prepared from deionized water. The electrodeposition of the Ni-Co electrocatalyst was carried out at a current density of 3~ 6A/dm^2 for 20 min. The bath temperature was maintained at 30~60℃, and the pH value was kept at 2 for the duration. Electrodeposition of the Ni-Co electrocatalyst was performed using a WY305digital DC current/ voltage-stabilized power. A digital PHS-3E precision pH meter was used to measure the pH value of the electrolyte, and the pH was adjusted to appropriate values by adding dilute hydrochloric acid or sodium hydroxide. The electrolyte was stirred by an 85-2 type digital constant temperature magnetic stirrer. After electrodeposition, the cathode surface was cleaned with deionized water, then the Ni-Co deposit with a thickness of 20~45μm was peeled off from the titanium substrate and dried for subsequent electrocatalytic HER experiments.

2.2 Microstructural analysis and electrochemical test

Prior to electrochemical evaluation, the surface morphology of Ni-Co samples was investigated by scanning electron microscopy (SEM) (JSM-6360LV, JAN), and their surface composition was examined by energy dispersive X-ray spectroscopy (EDS) (EDXGENESIS 60S，EDAXInC,USA) attached to the SEM. The crystalline structure of the deposited Ni-Co sample was determined by using an X-ray diffraction (XRD) (RigakuD/Max2500) at 40kv and 250mA using Ni filter and Cu α-radiation. The cathodic polarization curves, Tafel curves, cyclic voltammetry, electrochemical impedance spectroscopy (EIS) and chronoamperometry were measured by using a CHI660E electrochemical workstation (CH Instruments, Shanghai, CHN). A three -electrode H-type cell with three compartments was used to carry out all the electrochemical experiments. The Ni-Co deposit with a geometric area of 1cm^2 was used as the working electrode, a large area Pt plate served as the auxiliary electrode and a saturated calomel electrode (SCE) was used as the reference electrode. A Luggin capillary was used to reduce the liquid junction potential and the ohmic potential drop (*iR*) of the solution. All the electrochemical experiments in the water electrolysis for HER were carried out in solutions of sulfuric acid with concentrations of 0.0225~2.25M. The cathodic ploarization test for HER was performed at a scan rate of 1mV/s, and the scan rate of cyclic voltammetry was 10mV/s. Impedance tests were performed from frequencies of 100kHz to 0.005Hz, the open circuit potential was used as the initial potential, and the amplitude of the potential was kept at 5mV. Due to super toughness and excellent corrosion resistance, Ni-Co samples with compositions (wt%) of $Ni_{64.4}Co_{35.6}$, $Ni_{79.9}Co_{20.1}$ and $Ni_{82.5}Co_{17.5}$ were used as working electrodes and designated as electrode A, B and C. The samples were obtained at current densities of 3A/dm^2, 5A/dm^2 and 6A/dm^2, respectively. The HER tests were carried out at temperatures of 15~35℃.

3. RESULTS AND DISCUSSION

3.1 Characterization of Ni-Co electrocatalysts

The SEM images of the Ni-Co samples are shown in Fig.1. The surface of Ni-Co electrocatalyst is rough and silvery with no pinholes. Spherical protrusions, deposited particles with a relatively uniform diameter, are observed on each Ni-Co sample's surface, and there are distinct compact boundaries between each of the particles. Compared with smooth surface electrodes, the Ni-Co electrodes present a larger specific surface area, which favors the HER activity. In comparing the three Ni-Co electrodes in Fig. 1, it can be found that the surface displayed in Fig. 1(c) is relatively smooth, while the surface depicted in Fig. 1(b) is relatively rough, composed of numerous smaller spherical particles gathered tightly together exhibiting a fabric-like morphology. Fig.1(a), however, presents a rougher surface than that of either Fig. 1(b) or Fig. 1(c), showing that the surface roughness of a Ni-Co sample increases with the increase of cobalt content.

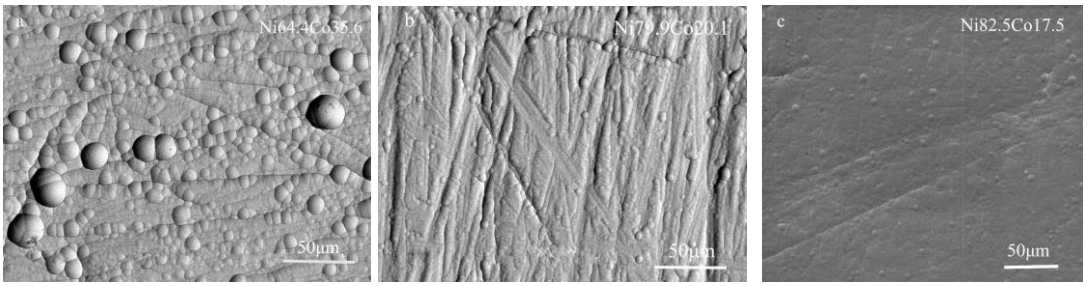

Figure 1. SEM images of Ni-Co (a-$Ni_{64.4}Co_{35.6}$ b-$Ni_{79.9}Co_{20.1}$ c-$Ni_{82.5}Co_{17.5}$).

The crystalline characteristics of the Ni-Co samples were confirmed by XRD. Fig.2 shows the XRD patterns of Ni-Co with the compositions of $Ni_{64.4}Co_{35.6}$, $Ni_{79.9}Co_{20.1}$ and $Ni_{82.5}Co_{17.5}$.

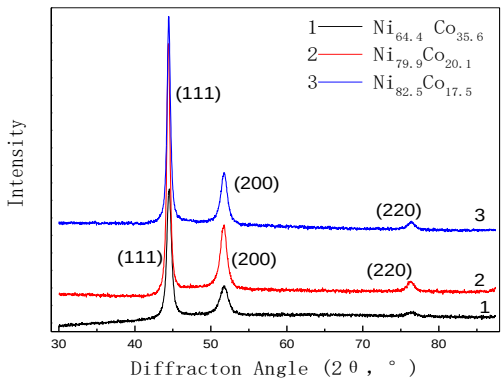

Figure 2. XRD patterns of Ni-Co with various compositions.

The XRD patterns of the three Ni-Co samples show that there are three obvious diffraction peaks such as (111), (200), (220) at around 2θ =44.377°, 51.708° and 76.153°. In particular, the predominant peak (111) and the second peak (200) are sharp and narrow, corresponding to the

characteristic peaks of nickel**.** The Ni-Co alloy forms only Ni matrix and the Co element becomes incorporated into the nickel matrix [26]. No separate peak for Co is found on the Ni-Co alloys, and no peak shift occurs in the XRD patterns, hence the Ni-Co electrocatalysts can be determined as the face centered cubic (fcc) solid solution.

3.2 HER activities of Ni-Co electrocatalysts

The cathodic polarization, electrochemical impedance and cyclic voltammetry techniques were used to investigate electrocatalytic behavior of Ni-Co electrocatalysts for HER. A comparative investigation on electrochemical performance of $Ni_{64.4}Co_{35.6}$ (electrode A), $Ni_{79.9}Co_{20.1}$ (electrode B) and $Ni_{82.5}Co_{17.5}$ (electrode C) was performed in a 0.225M H_2SO_4 aqueous solution at 15℃. Fig.3 shows the cathodic polarization curves for the above three Ni-Co samples. It can be seen from Fig.3 that the onset potential of HER for $Ni_{64.4}Co_{35.6}$, $Ni_{79.9}Co_{20.1}$ and $Ni_{82.5}Co_{17.5}$ is about -0.503V, -0.497V and -0.499V, respectively. It was reported that the onset potential of HER for Pt NFC (nanofoam catalyst) in 0.5 M H_2SO_4 is about -0.245Vvs.NHE (ca. -0.486Vvs.SCE)[31]. Although the concentration of the two H_2SO_4 solution**s** are quite different, the onset potential of electrode A, B and C in 0.225M H_2SO_4 are close to that of Pt NFC in 0.5 M H_2SO_4, illustrating their strong electrocatalytic activity for HER. However, with the decrease of Co content and the increase of Ni content in the Ni-Co, the cathodic polarization curves of HER gradually move toward the negative potential direction.

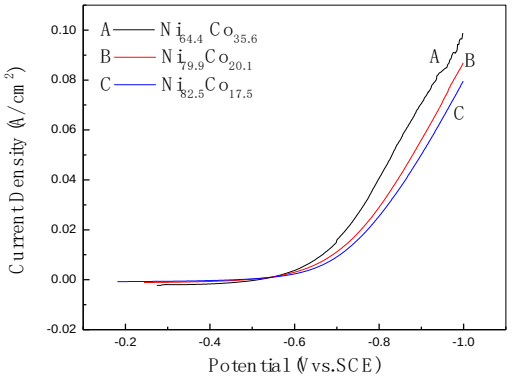

Figure 3. Cathodic polarization curves for Ni-Co in 0.225M H_2SO_4 at 15℃ (scan rate 1mV/s).

Among the three Ni-Co electrocatalysts, the $Ni_{64.4}Co_{35.6}$ shows the best HER activity. In comparison with the other two Ni-Co electrocatalysts, its cathodic polarization curve lies on the noblest potential direction with a lowest overpotential and a large cathodic current density. For example, to obtain the HER cathodic current density of 10mA/cm^2, the corresponding HER overpotential for $Ni_{64.4}Co_{35.6}$, $Ni_{79.9}Co_{20.1}$ and $Ni_{82.5}Co_{17.5}$ is 0.392V, 0.447V and 0.527V, respectively, illustrating the superior HER electrocatalytic activity of $Ni_{64.4}Co_{35.6}$ compared to the other two Ni-Co electrocatalysts. The better electrocatalytic HER activity of $Ni_{64.4}Co_{35.6}$ is attributed to an improvement in the surface roughness and the Co content.

Fig.4 shows the potentiodynamic polarization curves of $Ni_{64.4}Co_{35.6}$, $Ni_{79.9}Co_{20.1}$ and $Ni_{82.5}Co_{17.5}$. The corrosion potential (E_{corr}) and the corrosion current density (i_{corr}) obtained from the curves are shown in Table 1. The i_{corr} values of the three Ni-Co catalysts are all small, at the same 10^{-1} mA·cm^{-2} order of magnitude, which exhibits their better corrosion resistance and greater stability in acidic solution.

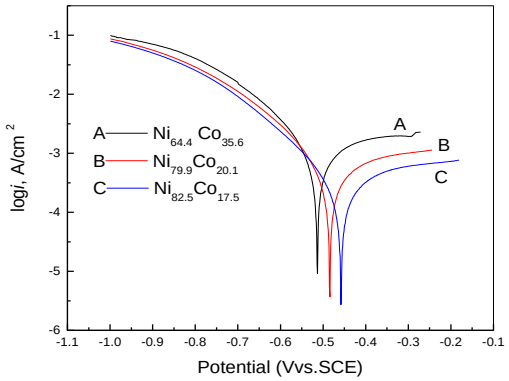

Figure 4. Potentiodynamic polarization curves in 0.225M H_2SO_4 at 15℃(scan rate 1mV/s).

The overpotential is almost linear with *logi* in the range of overpotential more than 100mV. By using linear fit, the kinetic parameters such as Tafel slope, intercept and exchange current density are derived from the Tafel equation (1) which is shown below

$$\eta = a + b\log i = -\frac{2.303RT}{\alpha zF}\log i_0 + \frac{2.303RT}{\alpha zF}\log i \qquad (1)$$

where η is the overpotential, a is the intercept, b is the Tafel slope, α is the charge-transfer coefficient, i is the current density, i_0 is the exchange current density. At the overpotential of 0.1V~0.2V, the parameters are summarized in Table 1.

Table 1. Kinetic parameters of Ni-Co for HER in 0.225M H_2SO_4 solution at 15℃

Catalyst	a,V	b,V dec^{-1}	i_0, mA/cm^2	E_{corr}, V	i_{corr}, mA/cm^2
$Ni_{64.4}Co_{35.6}$	0.493	0.165	1.03	-0.50	3.55×10^{-1}
$Ni_{79.9}Co_{20.1}$	0.536	0.173	7.98×10^{-1}	-0.49	2.58×10^{-1}
$Ni_{82.5}Co_{17.5}$	0.54	0.167	5.83×10^{-1}	-0.46	1.64×10^{-1}

The Tafel slope is an inherent property indicative of the electrocatalyst that is determined by the rate-limiting step of the HER [32]. It can be seen from Table 1 that the Tafel slope of electrodes $Ni_{64.4}Co_{35.6}$, $Ni_{79.9}Co_{20.1}$ and $Ni_{82.5}Co_{17.5}$ are 0.165, 0.173 and 0.167, respectively. Their slopes are close to each other, which shows that the mechanism of HER of these electrodes is basically the same. When the reaction mechanism is the same, the exchange current density can be used to measure the activities of electrodes for HER. The $Ni_{64.4}Co_{35.6}$ exhibits an apparent exchange current density of 1.03

mA/cm^2 which is 1.29 times that of $Ni_{79.9}Co_{20.1}$, and is 1.77 times that of $Ni_{82.5}Co_{17.5}$, showing, once again, that the $Ni_{64.4}Co_{35.6}$ with the highest Co content possesses the highest HER activity among the three Ni-Co samples. The i_0 values of some reported HER electrocatalysts in 0.5M H_2SO_4 are shown in Table 2.

Table 2. The i_0 value of some reported catalysts

Catalyst	Exchange current density i_0
Ni_2 P	0.033 mAcm $^{-2}$ [33]
Ni-Fe-P	0.316mAcm^{-2} [34]
$Ni_{76}Mo_{19}P_5$	1.86×10^{-1} mA/cm^2 [30]
NiMo,	2.7×10^{-2} mA/cm^2 [32]
Ni/C	1.8×10^{-3}mA/cm^2 [32]
Pt/C	3.2×10^{-1} mA/cm^2 [32]

It can be seen from Table 2 that the i_0 of $Ni_{64.4}Co_{35.6}$ in 0.225M H_2SO_4 is larger than that of some reported catalysts in 0.5M H_2SO_4, suggesting its higher activity towards HER.

The electrochemical impedance spectroscopy (EIS) technique was used to further examine the HER activity of various Ni-Co catalysts. The EIS of $Ni_{64.4}Co_{35.6}$, $Ni_{79.9}Co_{20.1}$ and $Ni_{82.5}Co_{17.5}$ in 0.225mol/l sulfuric acid solution at 15℃ with the initial potential kept at -0.161V is shown in Fig.5.

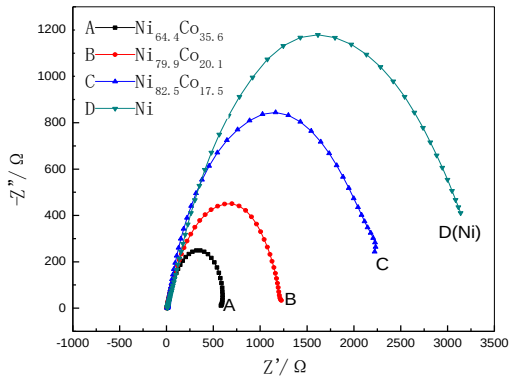

Figure 5. Impedance of Ni-Co in 0.225mol/l H_2SO_4 solution at 15℃ and -0.161V.

In the same frequency range, the EIS of the $Ni_{64.4}Co_{35.6}$, $Ni_{79.9}Co_{20.1}$ and $Ni_{82.5}Co_{17.5}$ electrodes are all semicircle arcs in the first quadrant, showing that the reaction mechanism of electrocatalytic HER on three different Ni-Co electrodes is the same. It is known that the mechanism of HER in acidic solution involves the formation of an adsorbed hydrogen intermediate M-H_{ads} (Volmer reaction，Eq(2)), followed by an electrochemical (Heyrovsky reaction, Eq(3)) and/or a chemical hydrogen desorption step (Tafel reaction, Eq(4))[24, 35].

$M + H^+ + e^- \rightarrow M\text{-}H_{ads}$ (Volmer reaction) (2)

$M\text{-}H_{ads} + H^+ + e^- \rightarrow H_2 + M$ (Heyrovsky reaction) (3)

$M\text{-}H_{ads} + M\text{-}H_{ads} \rightarrow H_2 + 2M$ (Tafel reaction) (4)

Fig. 5 shows that the resistance of the solution is very small, and there is no straight line at a 45° angle in the low frequency region, illustrating no concentration polarization of reactive ions occurs. The semicircle arc impedance complex plane plot shows that the polarization of the electrode potential is entirely generated by electrochemical steps. According to the literature of HER[20] and the Tafel slope shown in Table 1, *b* ranging from 0.165 to 0.173 V dec^{-1}, higher than 0.118V dec^{-1}, it can be derived that HER takes place by the Volmer- Heyrovsky mixing mechanism. It is known that the charge transfer process is the interface between electrocatalyst and electrolyte, which is attributed to a charge transfer resistance (*Rct*) and constant phase element (CPE) [36,37,38]. The semicircle diameter of EIS of the $Ni_{64.4}Co_{35.6}$, $Ni_{79.9}Co_{20.1}$, $Ni_{82.5}Co_{17.5}$ and Ni electrodes increases sequentially, which shows that the electrochemical reaction resistance (*Rct*) of the Ni-Co electrodes for HER is much less than that of the Ni electrodes. According to Engel Brewer's valence bond theory, the discharge of H_2O molecules requires paired d orbital electrons. Ni has a d^8 electronic structure that facilitates electron transfer to the H_2O molecule, which subsequently leads to the breaking of the O-H bond. Co has a d^7electronic structure that can provide the half empty d orbit, which is beneficial to the adsorption of H. Therefore, Ni and Co have a good electrocatalytic HER synergistic effect, and the electrocatalytic activity for HER of the Ni-Co electrode is better than that of the single metal Ni electrode. It can be seen that with the increase of Co content, the resistance of the Ni-Co electrode for HER decreases, and the $Ni_{64.4}Co_{35.6}$ electrode reveals a smaller electrochemical reaction resistance than the $Ni_{79.9}Co_{20.1}$ and $Ni_{82.5}Co_{17.5}$ samples. It is generally recognized that a smaller *Rct* value corresponds to faster kinetics [34]. It is therefore concluded that the electron transfer rate is faster and the cathodic efficiency is higher during the HER process for $Ni_{64.4}Co_{35.6}$.

Fig. 6 is the typical cyclic voltammograms (CV) for the electrode of $Ni_{64.4}Co_{35.6}$, $Ni_{79.9}Co_{20.1}$ and $Ni_{82.5}Co_{17.5}$ in 0.225M H_2SO_4 solution at 15℃.

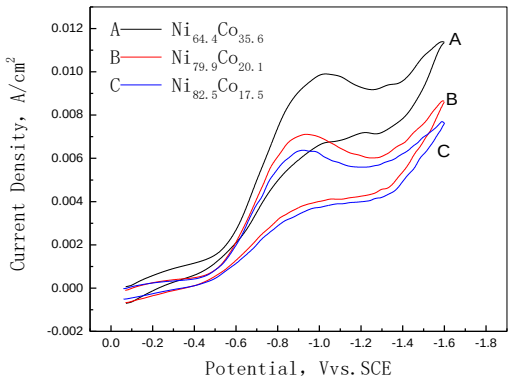

Figure 6. CV curves of Ni-Co in 0.225M H_2SO_4 solution at 15℃ (sacn rate 10mV/s).

As shown in Fig.6, there is only one peak for the three cases in the cathodic region and their shapes are approximately the same. The reduction peak potentials of the $Ni_{64.4}Co_{35.6}$, $Ni_{79.9}Co_{20.1}$ and $Ni_{82.5}Co_{17.5}$ electrodes are -1.11V, -0.92V and -0.902V, respectively. The reduction peak current density for electrode A, B and C is about 10mA/cm^2, 7mA/cm^2 and 6mA/cm^2, respectively, which is even far greater than that of $Pd_{65}Pt_{35}$ NFC in 0.5M H_2SO_4 at scan rate 10 mV/s [31]. It can be seen that

the reduction peak current density of the $Ni_{79.9}Co_{20.1}$ electrode is higher than that of $Ni_{82.5}Co_{17.5}$ electrode and lower than that of the $Ni_{64.4}Co_{35.6}$ electrode. Compared with the $Ni_{79.9}Co_{20.1}$ and the $Ni_{82.5}Co_{17.5}$ electrode, the HER potential of the $Ni_{64.4}Co_{35.6}$ electrode is the most positive, its HER current is the greatest and its cathodic reduction peak is the highest, which is consistent with the results obtained from cathodic polarization curves. In the reverse scanning process, at the electrode of $Ni_{64.4}Co_{35.6}$, $Ni_{79.9}Co_{20.1}$ and $Ni_{82.5}Co_{17.5}$ there begins to appear an oxidation current from -0.22V, -0.34V and -0.36V, respectively, which is due to the oxidation of the adsorbed hydrogen in the Ni-Co electrode. No obvious oxidation peaks are found on the anodic branch for the three electrodes, indicating that the Ni-Co alloy electrode has good stability and is not easily oxidized.

3.3 HER catalytic activities of Ni-Co at various temperature

The cathodic polarization and overpotential of $Ni_{64.4}Co_{35.6}$ at various temperature are shown in Fig.7(a) and Fig.7(b), respectively.

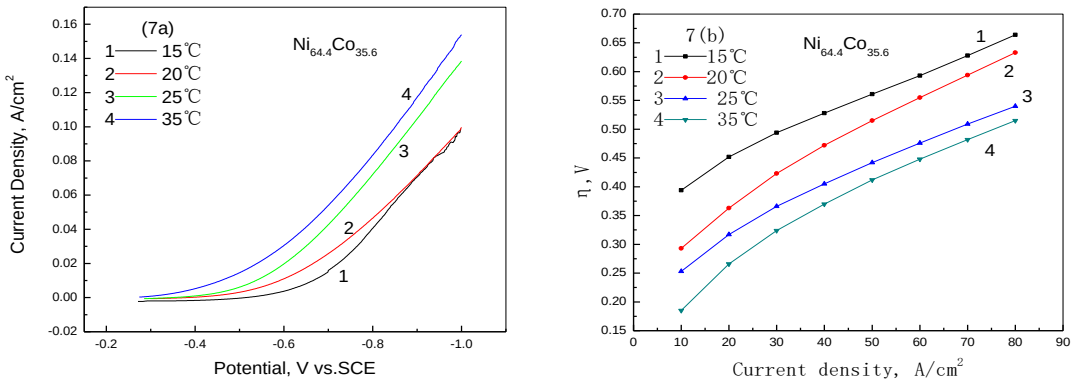

Figure 7. Polarization and overpotential of $N_{64.4}Co_{35.6}$ in 0.225M H_2SO_4 solution (scan rate 1mV/s).

Fig.7(a) shows that with the increase of temperature, the cathodic polarization curve shifts to the more positive potential direction, and the polarization of the HER decreases. Fig.7(b) illustrates that at the same overpotential, the reaction rate of HER corresponding to higher temperature is much higher than that at lower temperature. When the cathodic current density is 10mA/cm^2, the hydrogen evolution overpotential of electrode $N_{64.4}Co_{35.6}$ at temperatures of 15℃, 20℃, 25℃ and 35℃ is 0.39V, 0.29V, 0.25V and 0.24V, respectively. Therefore, the Ni-Co gives higher electrocatalytic activity at the higher temperature.

The EIS of $Ni_{64.4}Co_{35.6}$ in 0.225mol/l sulfuric acid solution at various temperatures is shown in Fig.8. It can be seen from Fig.8, that as the temperature is increased from 15℃ to 20℃, the semicircle diameter of EIS decreases dramatically, with the diameter at 20℃ about 0.83 times that of the diameter at 15℃. As the temperature is further increased from 20℃ to 25℃, 30℃ and 35℃, the diameter of the semicircle shows a corresponding decrease. The results again demonstrate that the electrochemical reaction resistance of the Ni-Co alloy electrode for HER decreases with the increase of temperature. Therefore, the temperature of about 35℃ is more beneficial to improve the electrocatalytic activity of Ni-Co for HER.

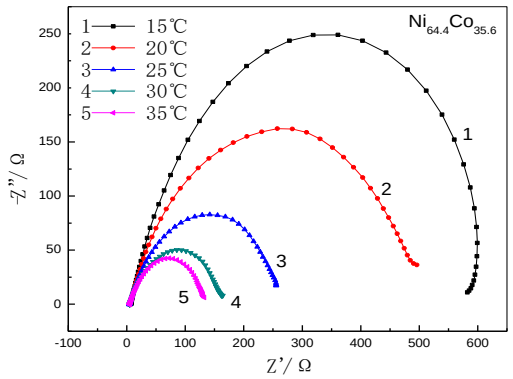

Figure 8. Impedance of $Ni_{64.4}Co_{35.6}$ in 0.225mol/l H_2SO_4 solution at -0.161V.

3.4 HER catalytic activities of Ni-Co in various H_2SO_4 solution

The activity of $Ni_{64.4}Co_{35.6}$ in various H_2SO_4 solutions is shown in Fig.9 and Fig.10, respectively.

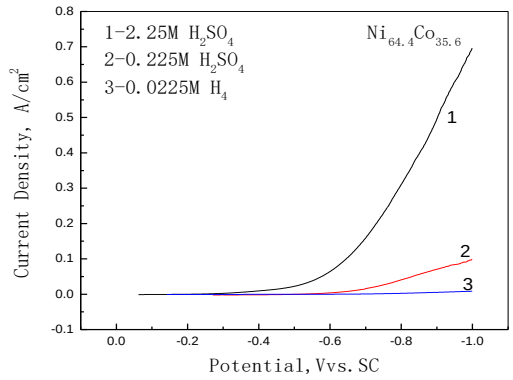

Figure 9. Polarization curves of $Ni_{64.4}Co_{35.6}$ in various H_2SO_4 solutions at 15℃.

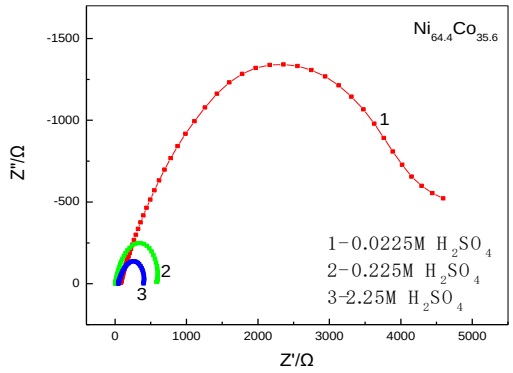

Figure 10. Impedance of $Ni_{64.4}Co_{35.6}$ in various H_2SO_4 solutions at 15℃ and at -0.161V.

Fig.9 shows that with the increase of concentration of H_2SO_4 solution, the cathodic polarization curve shifts markedly toward positive. At the current density of 10mA/cm^2, the overpotential in 0.0225M, 0.225M and 2.25M H_2SO_4 solution is 0.648V, 0.392V and 0.342V, respectively. It shows that the increase of the concentration of H_2SO_4 solution is beneficial in accelerating the rate of HER and decreasing the overpotential in the Ni-Co electrode. Fig.10 shows that with the increase of concentration of H_2SO_4 solution, the semicircle diameterof EIS is greatly decreased, which shows that the resistance of electrocatalytic HER is sharply reduced, and the electrocatalytic activity of Ni-Co electrode is greatly enhanced.

3.5 Stability of the Ni-Co electrocatalyst for HER

Stability is another key criterion to evaluate the properties of an electrocatalyst. The stability of $Ni_{64.4}Co_{35.6}$ for HER in H_2SO_4 solutions, especially at higher concentrations such as 2.25M was investigated by chronoamperometry. The chronoamperometric (CA) curve recorded at -0.6V in 2.25M H_2SO_4 at room temperature is depicted in Fig.11, indicating that there is no obvious drop in the current density even after 1000s. It can be noted that no obvious fluctuation phenomenon appears on the curve, thus showing that $Ni_{64.4}Co_{35.6}$ exhibits good steady state activity for electrolysis HER in an acidic environment. Even after 3 hours of hydrogen evolution reaction at the higher potential of -0.6V in 2.25M H_2SO_4, the mass of $Ni_{64.4}Co_{35.6}$ remains constant, further showing its considerable corrosion resistance and excellent long term electrocatalytic reaction durability in an acid medium.

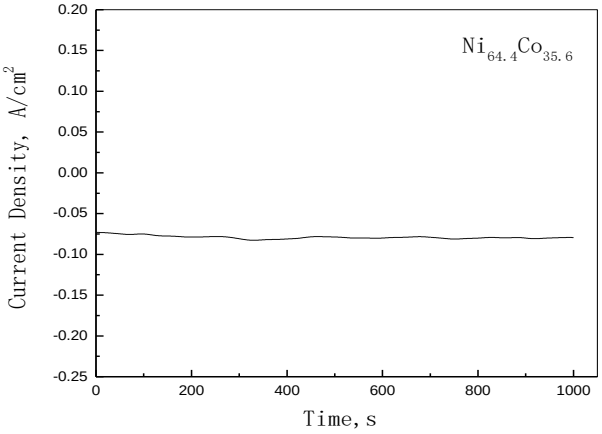

Figure 11. CA - curve for HER catalyzed by $Ni_{64.4}Co_{35.6}$ at -0.6V in 2.25M H_2SO_4 solution.

4. CONCLUSIONS

Ni-Co binary catalysts were synthesized by electrodeposition on titanium, and were characterized electrochemically for HER in a 0.225M H_2SO_4 solution, showing higher catalytic properties and better stability. The Ni-Co catalyst with 35.6wt% Co exhibits the highest catalytic activities for HER. The HER takes place by the Volmer- Heyrovsky mixing mechanism. By increasing

the temperature and concentration of the H_2SO_4 solution, the electrocatalytic activity of Ni-Co for HER is greatly enhanced.

ACKNOWLEDGEMENT
This work was financially supported by the Innovative project of Guangdong Education Department (2016KTSCX084), and Scientific research project of Hanshan Normal University(QD20150320).

References

1. K. Nath, M. M. Najafpour, R. A. Voloshin, S. E. Balaghi, E. Tyystjarvi, R. Timilsina, J. J. Eaton-Rye, T. Tomo, H. G. Nam, H. Nishihara, S. Ramakrishna, J. R. Shen, S. I. Allakhverdiev, *Photosynth. Res.*, 126 (2015) 237.
2. M. M. Najafpour, E. Amini, *Dalton Trans.*, 44 (2015) 154419.
3. M. M. Najafpour, S. Madadkhani, *Photosynth. Res.*, 130 (2016) 73.
4. M. M. Najafpour, B. Kaboudin, R. Mostafalu, M. Shahbazy, R. Safdari, M. Kompany-Zareh, *Int. J. Hydrogen Energy*, 42 (2017) 11187.
5. T. Wilberforce, Z. E. Hassan, F. N. Khatib, A. A. Makky, A. Baroutaji, J. G. Carton, A. G. Olabi, *Int. J. Hydrogen Energy,* 42 (2017) 25695.
6. V. V. Emets, I. I. Ponomarev, V. A. Grinberg, N. A. Mayorova, M. Y. Zharinova,Y. A. Volkova, E. A. Nizhnikovskii, K. M. Skupov, D. Yu. Razorenov, V. N. Andreev, I. I. Ponomarev, *Russ. J. Electrochem.*, 53 (2017) 86.
7. O. Emin, B. S. F. Gul, O. Osman, T. B. Erdor, C. Ekrem, K. Murat, K. Cigdem, C. Metin, T. Anilcan, Y. M. Suha, *Int. J. Hydrogen Energy*, 42 (2017) 691.
8. T. I. Okedi, Q. Meyer, H. M. A. Hunter, P. R. Shearing, D. J. L. Brett, *Int. J. Hydrogen Energy*, 42 (2017) 13850.
9. S. H. Chan, J. P. Stempien, O. L. Ding, P. C. Su, H. K. Ho, *Int. J. Hydrogen Energy*, 41 (2016) 13869.
10. T. T. Sun, J. Cao, J. Dong, H. Y. Du, H. J. Zhang, J. F. Chen, L. B. Xu, *Int. J. Hydrogen Energy*, 42 （2017）6637.
11. A. H. Zhang, S. J. Yu, Y. M. Jiang, L. P. Jia, X. H. Xia, W. C. Ye, C. M. Wang, *Int. J. Hydrogen Energy*, 40 (2015) 16238.
12. B. Rezaei, M. Mokhtarianpour, A. A Ensafi, *Int. J. Hydrogen Energy*, 40 (2015) 6754.
13. X. Zhao, X. Ma, J. Sun, D. H. Li, X. R.Yang, *ACS nano*, 10 (2016) 2159.
14. J. Kubisztal, A. Budniok, A. Lasia, *Int. J. Hydrogen Energy*, 32 (2007) 1211.
15. B. Subramanya, Y. Ullal, S. U. Shenoy, D. K. Bhat, A. C. Hegde, *RSC Adv.*, 5 (2015) 47398.
16. J. M. Jaksic, M. V. Vojnovic, N. V. Krstajic, *Electrochim. Acta*, 45 (2000) 4151.
17. N. V. Krstajic, V. D. Jovic, L. Gajic-Krstajic, B. M. Jovic, A. L. Antozzi, G. N. Martelli, *Int. J. Hydrogen Energy*, 33 (2008) 3676.
18. Q. Han, S. Cui, N. W. Pu, J. S. Chen, K. R. Liu, X. J. Wei, *Int. J. Hydrogen Energy*, 35 (2010) 5194.
19. S. H. Hong, S. H. Ahn, J. Choi, J. Y. Kim, H. Y. Kim, H. J. Kim, J. H. Jang, H. Kim, S. K. Kim, *Appl. Surf. Sci.*, 49 (2015) 629.
20. González-Buch, I. Herraiz-Cardona, E. Ortega, J. García-Antón, V. Pérez-Herranz, *Int. J. Hydrogen Energy*, 38（2013）10157.
21. C. Lupi, A. Dell'Era, M. Pasquali, *Int. J. Hydrogen Energy*, 34 (2009) 2101.
22. C. Fan, D. L. Piron, P. Paridis, *Electrochim. Acta*, 39 (1994) 2715.
23. C. Lupi, A. Dell'Era, M. Pasquali, *Int. J. Hydrogen Energy*, 39 (2014) 1932.
24. D. Gao, J. N. Guo, X. Cui, L. Yang, Y. Yang, H. C. He, P. Xiao, Y. H. Zhang, *ACS Appl. Mater. Interfaces*, 9 (2017) 22420.

25. F. Rosalbino, S. Delsante, G. Borzone, E. Angelini, *J. Alloys Compd.*, 429 (2007) 270.
26. J. Vijayakumar, S. Mohan, S. Anand Kumar, S. R. Suseendiran, S. Pavithra, *Int. J. Hydrogen Energy*, 38（2013）10208.
27. P. R. Zabinski, S. Meguro, K. Asami, K. Hashimoto, *Mater. Trans.*, 47 (2006) 2860.
28. N. Wang, T. Hang, D. W. Chu, M. Li, *Nano-Micro Lett.*, 7 (2015) 347.
29. C. G. Buch, I. H. Cardona, E. M. Ortega, J. G. Antón, *Chem. Eng. Trans.*, 32 (2013) 865.
30. G. J. Lu, P. Evans, G. Zangari, *J. Electrochem. Soc.*, 150 (2003) A551.
31. B. Rezaei, M. Mokhtarianpour, A. A. Ensafi, *Int. J. Hydrogen Energy*, 40 (2015) 6754.
32. Y. Zhang, Y. H. Wang, S. P. Jia, H. Q. Xu, J. B. Zang, J. Lu, X. P. Xu, *Electrochim. Acta*, 222 (2016) 747.
33. E. J. Popczun, J. R. McKone, C. G. Read, A. J. Biacchi, A. M. Wiltrout, N. S. Lewis, R. E. Schaak, *J. Am. Chem. Soc.*, 135 (2013) 9267.
34. Z. Z. Ma, R. X. Li, M. Wang, H. J. Meng, F. Zhang, X. Q. Bao, B. Tang, X. G. Wang, *Electrochim. Acta*, 219 (2016) 194.
35. A. Lasia, A. Rami, *J. Electroanal. Chem.*, 294 (1990) 123.
36. X. Wang, R. Su, H. Aslan, J. Kibsgaard, S. Wendt, L. Meng, M. Dong, Y. Huang, F. Besenbacher, *Nano Energy*, 12 (2015) 9.
37. D. H. Youn, S. Han, J. Y. Kim, J. Y. Kim, H. Park, S. H. Choi, J. S. Lee, *ACS Nano*, 8 (2014) 5164.
38. W. F. Chen, C. H. Wang, K. Sasaki, N. Marinkovic, W. Xu, J. T. Muckerman, Y. Zhu, R. R. Adzic, *Energy Environ. Sci.*, 6 (2013) 943.